Journal of Alloys and Compounds 513 (2012) 118–124

Contents lists available at SciVerse ScienceDirect

Journal of Alloys and Compounds

journal homepage: www.elsevier.com/locate/jallcom

Structural, optical and photoconductivity characteristics of manganese doped cadmium sulfide nanoparticles synthesized by co-precipitation method

Sheo K. Mishra [a], Rajneesh K. Srivastava [a,*], S.G. Prakash [a], Raghvendra S. Yadav [b], A.C. Panday [b]

[a] Department of Electronics & Communication, University of Allahabad, Allahabad 211002, India
[b] Nanophosphor Application Centre, Department of Physics, University of Allahabad, Allahabad 211002, India

ARTICLE INFO

Article history:
Received 24 June 2011
Received in revised form
28 September 2011
Accepted 3 October 2011
Available online 17 October 2011

Keywords:
CdS
XRD
Anomalous photoconductivity
PL
TEM

ABSTRACT

Mn-doped CdS nanoparticles (NPs) have been synthesized by co-precipitation method and effect of Mn concentration on the structural, photoluminescence and photoconductivity properties have been studied. The X-ray diffraction (XRD) patterns show that the synthesized NPs have a cubical (zinc blende) phase. The clear lattice fringes in the high-resolution transmission electron microscopy (HRTEM) image, and selected area electron diffraction (SAED) patterns with bright circular rings with spots further confirms cubical nature. The estimated average particle size is found to be ~3.1 nm by TEM image. UV–visible (UV–vis) absorption spectroscopy is used to calculate band-gap of material and blue shift in absorption peak indicates quantum size confinement effect. In photoconductivity study, variation of photocurrent with voltage on ln–ln scale is found to follow power law superlinearly due to injection of additional charge carriers from one of the electrodes. The growth and decay in photocurrent spectra exhibit anomalous behaviors which may be attributed to photo-induced chemisorptions of oxygen molecules on surface of NPs. A significant improvement in photocurrent has been observed in Mn-doped CdS NPs with concentration of Mn as 3 mol% as compared to un-doped CdS NPs. Photoluminescence (PL) spectra of un-doped as well as Mn-doped CdS NPs have one emission peak centered at ~526 nm whereas Mn-doped CdS NPs show one additional emission peak centered at ~575 nm which may be assigned to $^4T_1 \rightarrow {}^6A_1$ transitions of Mn^{2+}.

1. Introduction

Currently, a nanometer-sized material is a subject of intensive research for their potential applications in the fabrication of functional nanodevices [1–4]. Due to large surface to volume ratio and quantum confinement effects, the electronic, optical and magnetic properties of nanometer-sized materials get significantly altered as compared to their bulk counterparts. Nanometer-sized materials such as ZnO, ZnS, CdO and CdS have been successfully used in a number of applications such as transistor, light emitting diodes (LED) and nanolasers [1,2,5–7]. Among these II–VI semiconductor compounds, CdS is a direct band gap (~2.42 eV) semiconducting material with exciton binding energy as 28 meV [8]. It has promising applications in optoelectronics, solar cells, X-ray detectors and photoconductive devices [1–7,9]. Doping is one of the most intensively used methods to modify the luminescence, electrical and optical properties of semiconducting nanomaterials by introducing traps and discrete energy states in the band gap for the excited electrons. Doped II–VI semiconductor materials with transition metal ions (Cu, Fe, Co, Ag and Mn) have attracted researchers and scientific communities as their incorporation leads to tailored structural, optical and luminescence properties [10–12]. Mn-doped CdS NPs have got much attention due to modified structural, electrical and luminescence properties [13–19]. Un-doped as well as Mn-doped CdS NPs are synthesized by co-precipitation method, sonochemical method, sol–gel method and reveres micelles method, etc. [14–20]. Co-precipitation method is simple, inexpensive and high yield producing method. In the present work, we have synthesized CdS and Mn-doped CdS nanoparticles by co-precipitation method and structural, photoluminescence and photoconductivity properties have been investigated. Photoconductive materials usually exhibit an increase in conductivity under illumination which is a direct result of the absorption of photon energy greater than band-gap of material. This phenomenon is known as positive photoconductivity. Though most of semiconductors are found to exhibit positive photoconductivity [21–28], there are several reports on anomalous photoconductivity (APC) wherein the conductivity decreases even under steady illumination. ZnO nanowire and nanoparticles, Co-doped ZnO nanobelts, TiO_2 nanocrystalline, CeO_2 NWs, ZnO NPs in a SiO_2 matrix, PVA capped ZnO NWs in air [29–38], etc. have been reported to exhibit

* Corresponding author. Tel.: +91 9415254349.
E-mail addresses: rkumarsau@gmail.com, sheokumarmishra@gmail.com (R.K. Srivastava).

0925-8388/$ – see front matter © 2011 Elsevier B.V. All rights reserved.
doi:10.1016/j.jallcom.2011.10.003

anomalous photoconductivity. The synthesized CdS and Mn-doped CdS NPs are found to exhibit anomalous photoconductivity.

2. Experimental

2.1. Chemicals

Cadmium acetate dehydrate ($Cd(CH_3COOH)_2{\cdot}2H_2O$), sodium sulfide ($Na_2S$), manganese acetate ($Mn(CH_3COO)_2{\cdot}4H_2O$) are procured from E. Merk Ltd. Mumbai, India. All the chemicals are of high purity (99.999%) and are A.R. grade. These are used directly without any special treatment.

2.2. Sample preparation

In a typical experiment, cadmium acetate dehydrate ($Cd(CH_3COOH)_2{\cdot}2H_2O$) is mixed in 50 ml of ethanol. In the above 50 ml solution, aqueous solution of sodium sulfide (Na_2S) is added drop wise to form CdS NPs. Manganese acetate ($Mn(CH_3COO)_2{\cdot}4H_2O$) is used with cadmium acetate ($Cd(CH_3COOH)_2{\cdot}2H_2O$) to prepare Mn-doped CdS NPs. Finally, the obtained product is washed with ethanol several times and is dried in vacuum oven at 40 °C for 4 h.

2.3. Instrumentation

The crystal structures of un-doped as well as Mn doped CdS NPs have been characterized by X-ray diffraction (XRD), using Rigaku D/MAX- 2200H/PC, Cu Kα (~1.5404 Å) radiation. Techni-G20 Stwin Transmission Electron Microscope has been used for recording TEM image. UV–visible absorption spectrum has been recorded using Perkin Elmer LS-35 spectrometer. The FTIR spectrum has been recorded on ABB FTLA 2000 FTIR spectrometer (Canada) in the wavenumber range of 4000–500 cm^{-1} on pellets obtained by mixing the sample in KBr. For photoconductivity measurements, a cell type device is used. The cell is formed by putting a thick layer of powdered sample in between two Cu electrodes having a spacing of 1 mm. The powdered layer is pressed with a glass plate for providing illumination area of 0.25 cm^2. The cell is mounted in a dark chamber. The light illumination is allowed to fall over the cell with a slit. The Hg lamp of 300 W is used as photo-excitation source at 490 nm excitation wavelength. A stabilized dc field (50–500 V/cm) is applied across the cell. For dark-current versus voltage (I_{dc}–V) measurements, the cell is first kept in the dark for several hours. Voltage dependence of dark-current and photocurrent is measured using a digital dc nano-ammeter. The time-resolved rise and decay of photocurrent spectra are recorded using RISH Multi 15S with adapter RISH Multi SI-232. The spectral response of photocurrent is measured at a fixed bias voltage of 30 V by illuminating the cell with wavelengths of visible light using a set of filters (405 nm, 436 nm, 490 nm, 546 nm, 580 nm, 610 nm and 691 nm) and an Hg lamp source of 300 W. All the observations have been recorded at room temperature in ambient air.

3. Results and discussion

3.1. Structural study

Fig. 1(a) shows XRD patterns of un-doped CdS as well as Mn-doped CdS NPs. XRD patterns are broadened as compared to those of bulk CdS which is confirmation of nano-sized particles formation. All the peaks corresponding to (1 1 1), (2 2 0), (3 1 1) of un-doped as well as Mn-doped CdS can be indexed to cubical zinc blend structure [37–41]. The lattice constants ($a = c$) are calculated for the most prominent peaks (Table 1) which are found to be close to standard values for the CdS phase in the JCPDS data (JCPDS card no: 10-454) [42]. The lattice parameters for the cubical zinc blend phase are calculated using formula [43] $(1/d^2) = (h^2 + k^2 + l^2/a^2)$ where 'a' is lattice parameter, d_{hkl} is the interplaner separation corresponding to Miller indices (h, k and l) which are given in Table 1. The average crystallite size (D) of un-doped as well as Mn-doped CdS NPs is estimated using Scherer's formula [43,44] $D = (0.9\lambda/\beta\cos\theta)$ where, D is crystallite size, λ is X-ray wavelength of Cu Kα radiation, β is full width at half maxima [FWHM] in radians, and θ is Bragg's angle. The estimated average crystallite size of these NPs is given in Table 1. No diffraction peak associated with Mn related compounds is observed which may be due to low Mn concentration. It is found that the variation in the lattice constants of Mn-doped CdS NPs are different as compared to that of un-doped CdS NPs which may be attributed to difference in ionic radii of Cd and Mn ($r^{2+}_{Cd} = 0.98$ Å and $r^{2+}_{Mn} = 0.66$ Å). Variation of crystallite

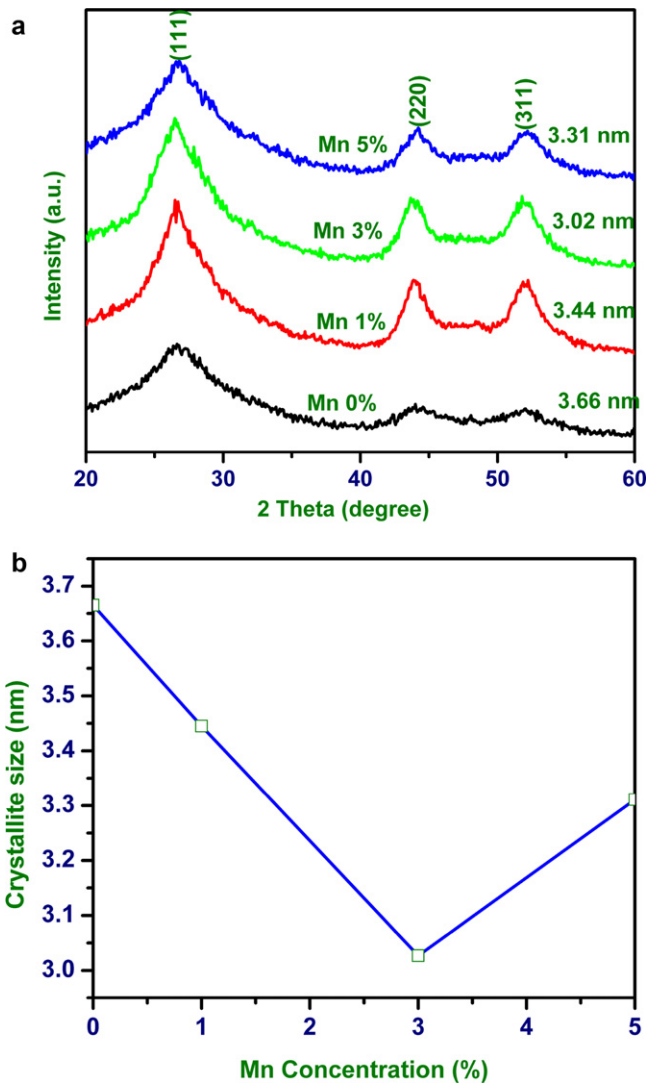

Fig. 1. (a) Powder XRD pattern of un-doped and Mn-doped CdS NPs with different doping levels of Mn, (b) variation of crystallite size of CdS:Mn NPs with different Mn doping levels.

size determined by Scherer's formula with different Mn concentrations is shown in Fig. 1(b). It is found that the CdS:Mn (1 mol%) NPs are smaller than un-doped CdS NPs. CdS:Mn (3 mol%) NPs are of reduced size as compared to CdS:Mn (1 mol%). At high concentration of Mn, CdS:Mn (5 mol%) are found to be larger than CdS:Mn (3 mol%). At low concentration, Mn^{2+} ions replace Cd^{2+} ions inside the nanoparticles. As the radius of Mn^{2+} ion (0.66 Å) is smaller than that of Cd^{2+} (0.98 Å), the size of nanoparticles reduces. If Mn concentration is increased further, the Mn^{2+} ions start replacing Cd^{2+} ions residing at surface of the nanoparticles which further reduces the size of nanoparticles. At high concentration of Mn (5 mol%), Mn^{2+} ions are supposed to reside on the surface forming Mn–Mn complexes. As Mn^{2+} ions are not replacing any Cd^{2+} ions, the size of the nanoparticles increases.

3.2. Morphology study

The morphology of CdS:Mn (3 mol%) NPs having particle sizes 2–5 nm are shown in Fig. 2(A). It is well evident that the particles are spherical in nature with little agglomeration and good crystallinity. Fig. 2(B) exhibits the particle size distribution histogram and corresponding Gaussian curve

Table 1
The 2θ values corresponding to peaks, d-spacing of the planes, miller indices, average crystallite size, and lattice constants.

Mn-doping in CdS	Positions [2θ]	d-Spacing [Å]	$h\,k\,l$	Average crystallite size (nm)	$a = c$ [Å]
0 mol% Mn	26.640	3.343	1 1 1	3.66 ± 1.12	5.79024
–	43.987	2.057	2 2 0		–
–	52.041	1.756	3 1 1		–
1 mol% Mn	26.492	3.362	1 1 1	3.44 ± 0.98	5.82314
–	43.883	2.061	2 2 0		–
–	52.218	1.750	3 1 1		–
3–mol% Mn	26.478	3.363	1 1 1	3.02 ± 1.15	5.82488
–	43.676	2.071	2 2 0		–
–	52.135	1.753	3 1 1		–
5 mol% Mn	26.561	3.353	1 1 1	3.31 ± 0.92	5.80756
–	44.215	2.007	2 2 0		–
–	52.188	1.751	3 1 1		–

fitting of CdS:Mn (3 mol%) NPs. An average particle size of 3.08 ± 0.053 nm is determined from particle size histogram. HRTEM image and selected-area electron differaction (SAED) pattern (Fig. 2C and D) indicate that the Mn-doped CdS NPs are cubical (zinc blende) polycrystalline material with diffuse halo type pattern, which are indicative of the reduction of particles (small size). The SAED patterns is used to know the type of crystalinity, i.e., single crystalline, polycrystalline and difuse

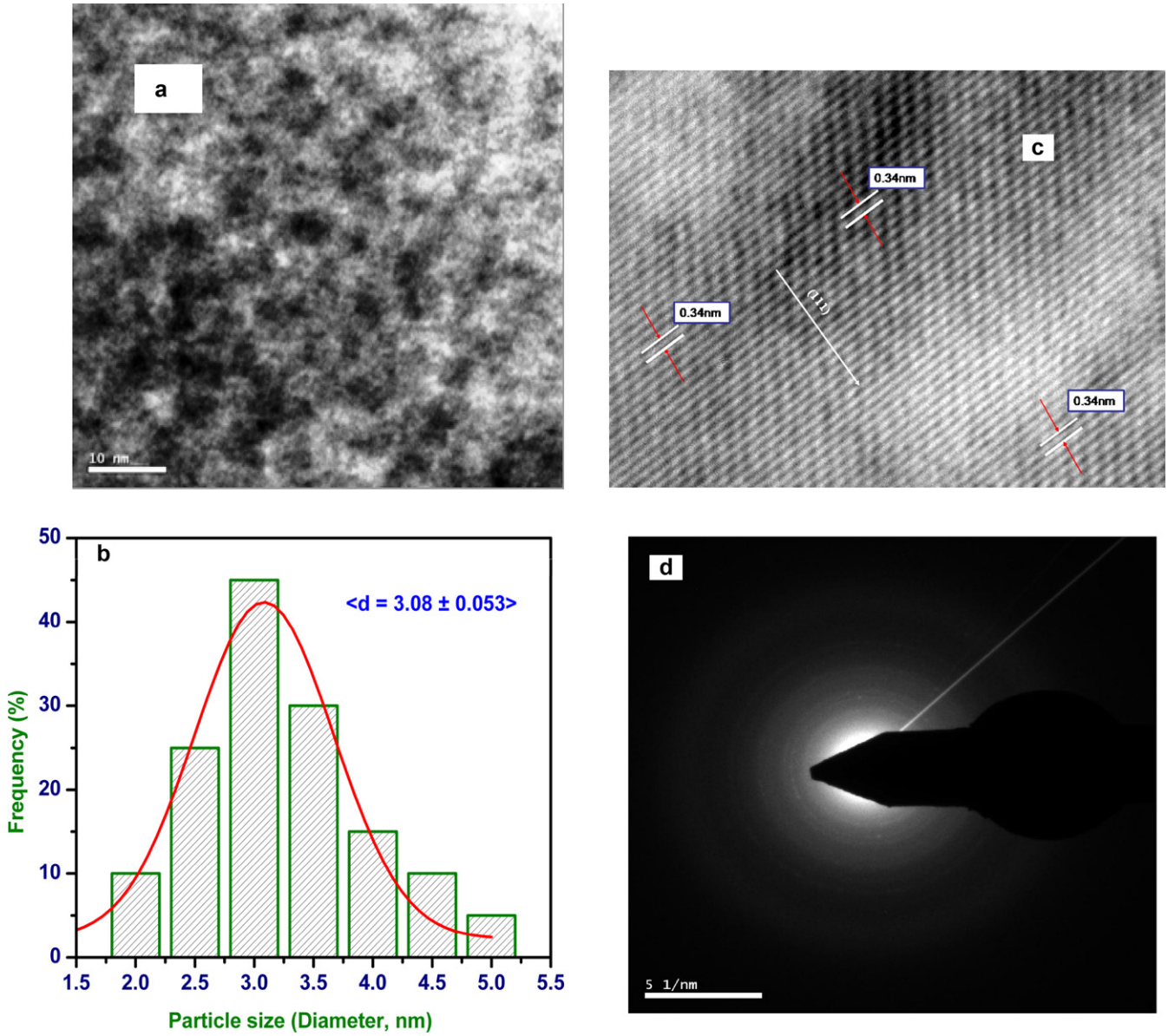

Fig. 2. (a) TEM image of CdS:Mn (3 mol%) NPs synthesized by co-precipitation method, (b) histogram representation of particle size distribution and corresponding Gaussian curve fit, (c) high resolution TEM (HRTEM) image and (d) selected area electron diffraction (SAED).

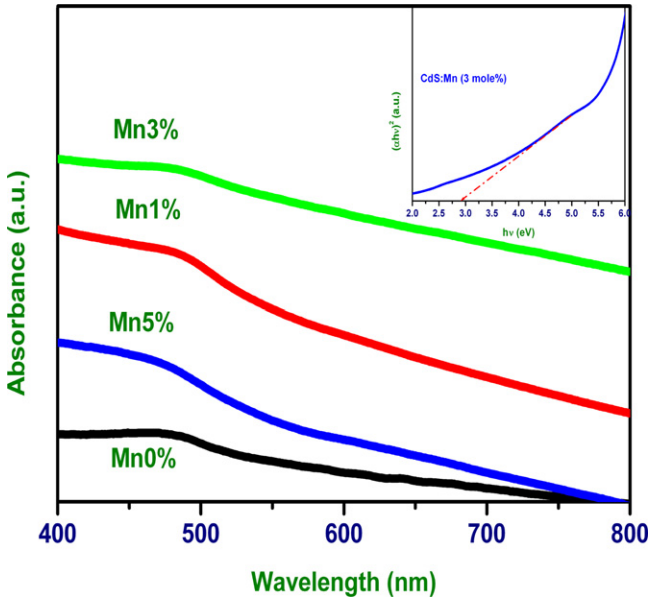

Fig. 3. UV–visible absorption spectrum of un-doped and Mn-doped CdS NPs synthesized by co-precipitation method. The inset shows plot of $(\alpha h\nu)^2$ vs. $(h\nu)$ CdS:Mn (3 mol%).

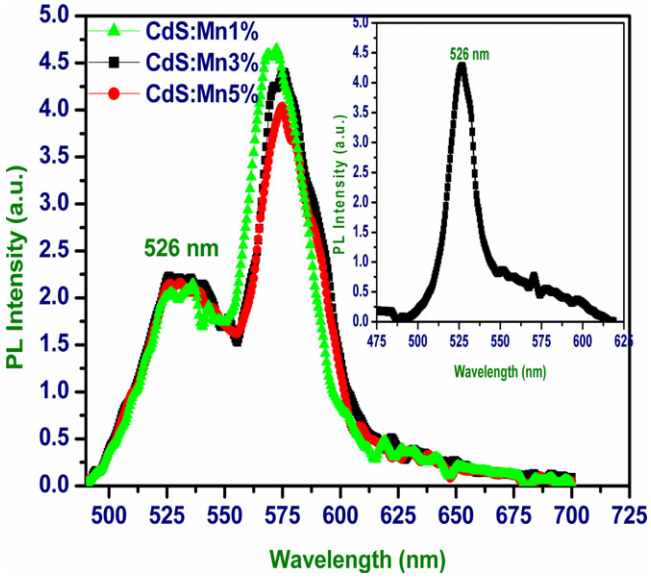

Fig. 4. PL spectra of Mn-doped CdS NPs synthesized by co-precipitation method. The inset shows the PL spectrum of un-doped CdS NPs.

polycrystalline-textured similar to amorphous nature [45,46]. The estimated average particle size of these spherical NPs (3.08 ± 0.053 nm) from histogram is similar to those obtained by XRD.

3.3. UV–vis absorption spectra study

The UV–vis absorption spectra of un-doped as well as Mn-doped CdS NPs are shown in Fig. 3. The absorption edge of bulk CdS is reported as 512 nm (2.42 eV) [47] while that of un-doped as well as Mn-doped CdS NPs is found at lower wavelengths. The absorption coefficient (α) is calculated using absorption data and formula [47] $\alpha = A\,(h\nu - E_g)^n/h\nu$ where, A is a constant, E_g is optical band gap of the material and n depends on the type of transition. In our case we have direct allowed transitions with $n = 0.5$. The optical band gap is determined by extrapolating the plot of $(\alpha h\nu)^2$ vs. $h\nu$, which is found to be 2.91 eV for CdS:Mn (3 mol%) as shown in inset of Fig. 3. Particle size of CdS:Mn (3 mol%) is calculated using effective mass approximation (EMA) formula [48,49]: $\Delta E_g = \left[\frac{\hbar^2\pi^2}{2\mu d^2}\right] - \frac{1.8e^2}{Pd} - 0.248E_R$

where $\Delta E_g = E_n - E_b$ is change in band gap due to quantum confinement, E_n and E_b are band gaps of nano and bulk CdS respectively, E_R is effective Rydberg energy, d is particle radius, P is permittivity of space with value as 5.5, μ_m is the combined effective mass of electrons and holes ($1/\mu_m = 1/m_e + 1/m_h$). The values of effective mass of electron and hole in CdS nanoparticles are approximatly 0.19 m_0 and 0.8 m_0 respectively, where m_0 is free electron mass. The first term in the EMA equation represents the electron–hole pair confinement kinetic energy, the second term is Coulomb interaction energy between electron and hole, and the last term is the result of the correlation effect. The calculated particle radius of CdS:Mn (3 mol%) NPs is found to be around 2 nm which is very close to particle size estimated by TEM micrograph as well as by XRD. As the Bohr exciton radius for CdS is 5.8 nm [40], this result is an evidence of strong quantum confinement in Mn-doped CdS NPs and is indicative of increase in band gap with decrease in particle size. In semiconductor materials confinement effects are strong for the particle having radius r, significantly smaller than the Bohr exciton radius, i.e., $r \ll a_B$, and intermediate confinement for those having $r \sim a_B$ while weak confinement for the particles having radius few times larger than Bohr radius, a_B, i.e., $r \gg a_B$.

3.4. Photoluminescence study

In photoluminescence, an electron excited by photon of fixed energy undergoes radiative recombination either at valence band, i.e., band edge emission or at surface/trap states within the forbidden gap [50]. In CdS NPs, the possible defects are cadmium vacancies (V_{Cd}), sulfur vacancies (V_s), cadmium interstitials (I_{Cd}^+) and sulfur interstitials (I_s^-) [15,20]. Fig. 4 shows the photoluminescence spectra of undoped as well as Mn-doped CdS NPs at room temperature with excitation wavelength of 437 nm. The PL spectrum of CdS NPs shows emission peak at ~526 nm (~2.35 eV). However, Mn-doped CdS NPs exhibit two major emission peaks, a broad emission peak centered around at ~526 nm (~2.35 eV) and one emission peak at ~575 nm (~2.15 eV). The green emission at ~526 nm is due to radiative recombination of electrons and holes via the surface/defect states present in the NPs [50,51]. The reduced PL intensity of green emission indicates transfer of energy from excited carriers trapped at the surface to Mn^{2+} ions. The orange emission ~575 nm is due to $^4T_1 \rightarrow {}^6A_1$ transition of Mn^{2+} [15,20,50–54]. Maximum orange emission intensity is found for 1 mol% Mn concentration. Orange emission intensity decreases when the Mn^{2+} content is increased beyond this limit, which may be attributed to Mn–Mn interactions. Taguchi et al. [55] has also reported that at high concentration (above 2–3 mol% Mn ions), Mn–Mn interactions cause reduction in luminescence activities. Variation as slight reduction in intensity of emission at ~575 nm is being accompanied by a small increase in intensity of emission at ~526 nm. High concentration of Mn doping helps formation of defect states responsible for emission at ~526 nm.

3.5. Photoconductivity study

3.5.1. Voltage dependence of photocurrent

Fig. 5 shows variation of photocurrent with applied voltage for un-doped CdS as well as Mn-doped CdS NPs on ln–ln scale. The variation of photocurrent, I_{pc} with applied voltage is found to have two straight line segments for both un-doped CdS as well as Mn-doped CdS NPs and can be expressed by power law,

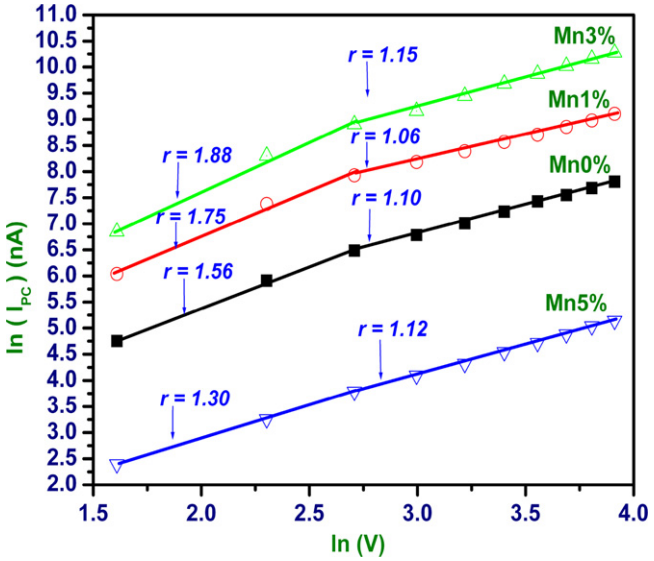

Fig. 5. Variation of photocurrent with voltage on ln–ln scale for un-doped and Mn-doped CdS NPs at room temperature.

$I \propto V^r$, where 'r' represents slope of each segment. Both segment of photocurrent for un-doped as well as Mn-doped CdS NPs show superlinear behavior ($r > 1$). It indicates that the additional charge carriers are being injected from one of the electrodes [54–57].

3.5.2. Time-resolved photocurrent rise and decay spectra

The doping effect of Mn has been studied by investigating the time-resolved rise and decay of photocurrent spectra of CdS NPs. Fig. 6(a) shows the rise and decay of photocurrent spectra for un-doped as well as Mn-doped CdS NPs, measured at room temperature under visible illumination (490 nm). The variation of dark-current with time before light illumination for un-doped and Mn-doped CdS NPs is shown in Fig. 6(b). The dark-current is measured until it gets stabilized. CdS NPs are usually n-type semiconductors due to sulfur vacancies and other native defects. These vacancies and native defects act as active sites for the adsorption of oxygen and water molecules. These surface-adsorbed oxygen and water molecules largely affect the dark and photoconductivity behavior of nanostructured materials because of their high surface to volume ratio [26]. The increase or decrease in dark-conductivity depends on the dominance of one of the two processes, i.e., adsorption of oxygen and desorption of oxygen. Oxygen molecules are first physically adsorbed onto the CdS NPs surface and then the chemisorptions process takes place by capturing free electrons. The process of adsorption of O_2 may be represented by $O_2 + 4e^- = 2O^{2-}$, that creates a depletion layer in the near-surface region of the nanoparticles resulting in a decrease in free charge carriers [58]. On the contrary free charge carriers increases due to desorption of O_2. In un-doped CdS as well as Mn-doped CdS NPs, dark current is initially high, which may be attributed to field induced desorption of oxygen molecules because the electric field appears to assist the process of desorption of oxygen [59,60]. With time dark current decreases and eventually it gets stabilized. This decrease in dark-conductivity is ascribed to dominance of the process of chemisorptions of oxygen after initial dominance of the process of field-assisted desorption of oxygen [59,60]. The stabilized dark-current in CdS:Mn (1 mol%) and CdS:Mn (3 mol%) NPs are higher than dark-current found in un-doped CdS NPs. In CdS:Mn (5 mol%) NPs, this is close to stabilized dark-current in un-doped CdS NPs. After doping of Mn, dark-conductivity in CdS:Mn (1 mol%) increases due to increase in thermally activated free carriers released from defect states introduced by incorporation of Mn inside the CdS NPs. At higher

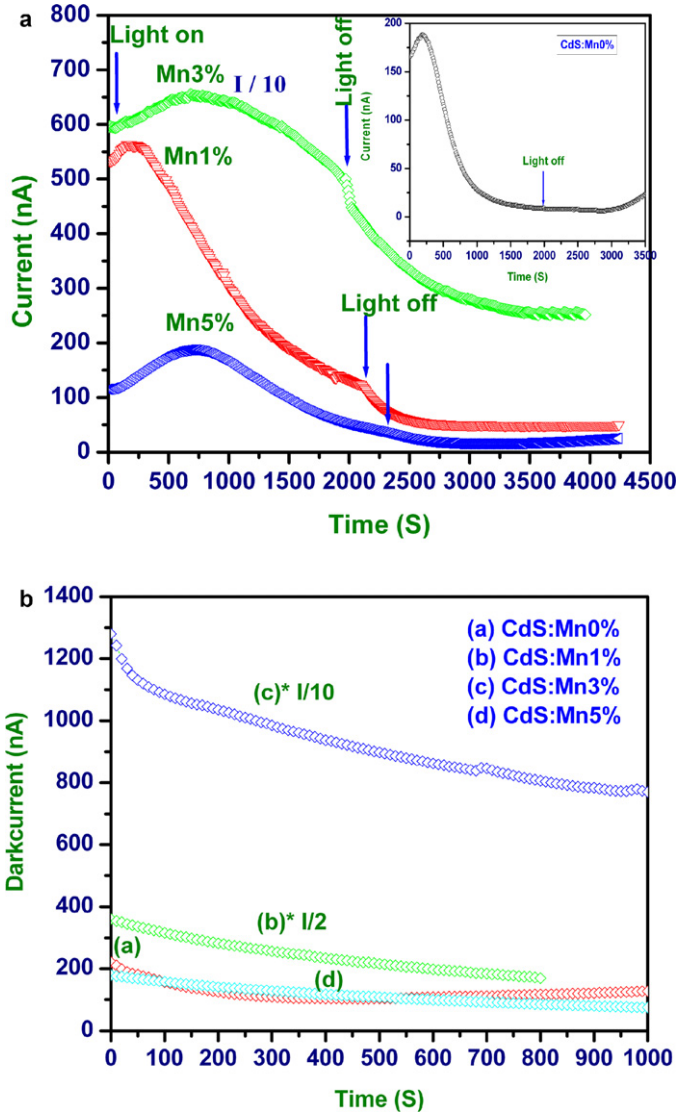

Fig. 6. (a) Time-resolved rise and decay photocurrent spectra of Mn-doped CdS NPs (inset figure shows rise and decay photocurrent spectrum of CdS NPs), (b) variation of dark-current with time before illumination.

concentration of Mn (3 mol%), more defect states are introduced contributing more to the dark-conductivity. When concentration of Mn is high (5 mol%), due to Mn–Mn interaction, concentration of defect states are supposed to get reduced thereby reducing the dark-conductivity in CdS:Mn (5 mol%) [55]. When the visible light is switched on, free carriers are generated due to absorption of photons of sub band-gap energy causing increase in current. Initial value of photocurrent in CdS:Mn (1 mol%) and CdS:Mn (3 mol%) NPs are higher than photocurrent found in un-doped CdS NPs. In CdS:Mn (5 mol%) NPs, this is close to the initial value in un-doped CdS NPs (Table 2). Variation of initial value of photocurrent

Table 2
Maximum dark-current, stabilized dark-current before light is switched on, and maximum photocurrent of un-doped and Mn-doped CdS NPs.

Mn-doping in CdS	Max. dark-current (nA)	Stabilized dark-current (nA)	Max. photocurrent (nA)
0 mol% Mn	240	130	196
1 mol% Mn	750	360	575
3 mol% Mn	12,500	6200	6800
5 mol% Mn	190	90	200

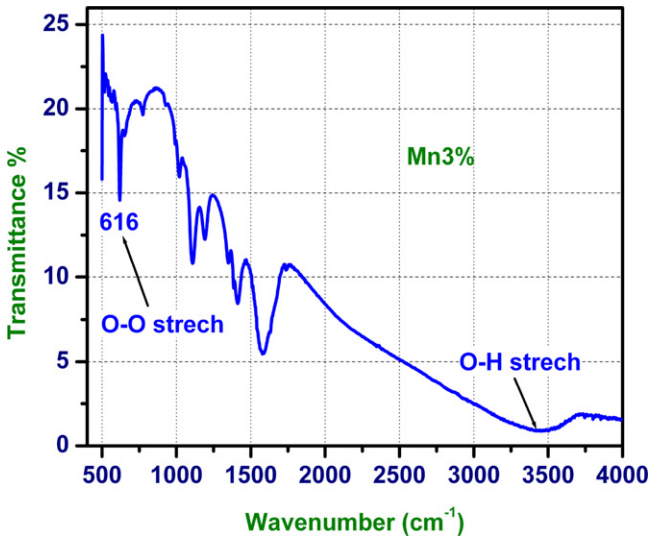

Fig. 7. FTIR spectrum of CdS:Mn (3 mol%) nanoparticles.

with concentration of Mn is associated with variation of dark-current in Mn-doped CdS NPs. All the samples are found to exhibit anomalous photoconductivity wherein the photocurrent decreases under steady illumination. With time, photocurrent drops below the stabilized dark-current resulting in negative photoconductivity (NPC). Such anomalous photoconductivity may be attributed to dominance of the process of photo-induced chemisorptions of oxygen molecules. The anomalous photoconductivity may also be attributed to photo-induced desorption of chemisorbed water molecules [61]. Peng et al. [34] have reported similar anomalous behavior of photocurrent in Co-doped zinc-oxide nanobelts and explained it on the basis of photo-induced desorption of chemisorbed water molecules. The presence of oxygen and water molecules on the surface of Mn-doped CdS NPs is confirmed by FTIR analysis of Mn-doped CdS NPs as shown in Fig. 7. A series of absorption peaks from 500 to 4000 cm^{-1} can be found, corresponding to the vibration mode of adsorption. Peaks between 600 and 800 cm^{-1} are due to oxygen stretching vibration. It is well-known that oxygen adsorbs on the surface in several forms like O_2, O_2^{2-}, O_2^-, O^-, and O^{2-} depending on the adsorption capability of semiconductor and experimental conditions [62]. A broadband at 3200–3600 cm^{-1} is assigned to the O–H stretching mode of hydroxyl group [63].

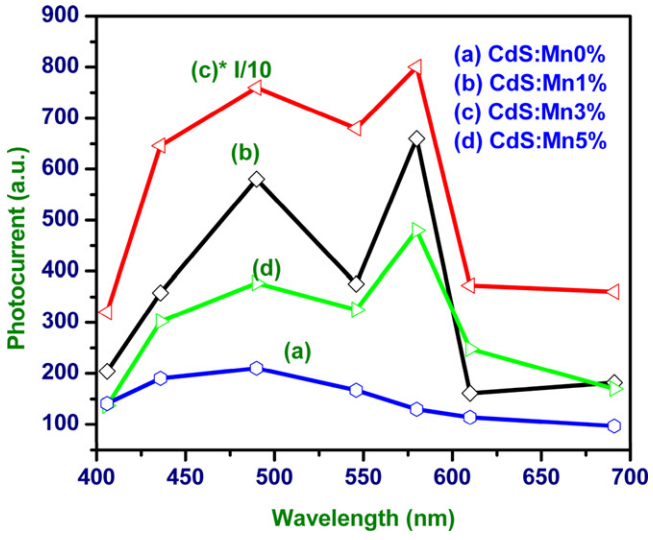

Fig. 8. Spectral response of un-doped and Mn-doped CdS NPs synthesized by co-precipitation method.

3.5.3. Spectral response of photocurrent

Fig. 8 shows the wavelength-dependent photocurrent spectra of un-doped as well as Mn-doped CdS NPs by illuminating the samples with light in visible range (400–700 nm). Photocurrent spectra of un-doped CdS and Mn-doped show a broad band from 450 to 550 nm which is consistent with the UV–visible absorption spectra (Fig. 3). Photocurrent spectra of Mn-doped CdS NPs show an additional band from 550 to 580 nm, which may be attributed to defect states due to doping of Mn.

4. Conclusions

We have studied photoconductivity and photoluminescence properties of un-doped as well as Mn-doped CdS NPs with particle size lying in the range of 2–5 nm synthesized by co-precipitation method. XRD, TEM and HRTEM patterns of CdS:Mn NPs confirm the cubical structure with good crystallinity. High-resolution TEM images show clear lattice fringes. The Bright rings and discrete light spots in selected area electron diffraction (SAED) patterns reveal diffuse polycrystalline-textured cubic nature. UV–visible absorption spectra of un-doped as well as Mn-doped CdS NPs show blue shift as compared to their bulk counterpart. Both un-doped as well as Mn-doped CdS NPs show PL emission peak centered at around 526 nm. This green emission may be due to radiative recombination of electrons and holes via surface or defect states present in the NPs. The Mn-doped CdS NPs exhibit one additional emission peak centered at around 575 nm which is attributed to $^4T_1 \rightarrow {}^6A_1$ transitions of Mn^{2+}. Un-doped as well Mn-doped CdS NPs are found to exhibit an anomalous photoconductivity which may be attributed to dominance of the process of photo-induced chemisorption of oxygen molecules on surface of NPs. Improvement in photocurrent has been observed in CdS:Mn (3 mol%) nanoparticles which is one order of magnitude higher as compared to photocurrent in un-doped CdS NPs.

Acknowledgement

The author Rajneesh K. Srivastava is thankful to UGC for its financial assistance in form of a project 37-395 (2009) (S.R.).

References

[1] G.F. Zheng, W. Lu, C.M. Lieber, Adv. Mater. 21 (2004) 1890.
[2] Y. Huang, H.F. Duan, C.M. Lieber, Small 1 (2005) 142.
[3] W.I. Danaher, L.E. Lyous, G.C. Morries, Sol. Energy Mater. 12 (1985) 137.
[4] X.T. Zhou, J.Q. Hu, C.P. Li, D.D.D. Ma, C.S. Lee, S.T. Lee, Chem. Phys. Lett. 369 (2003) 220.
[5] A.V. Maslov, C.Z. Ning, Appl. Phys. Lett. 83 (2003) 1237.
[6] Y.K. Liu, J.A. Zapien, C.Y. Geng, Y.Y. Shan, C.S. Lee, Y. Lifshitz, S.T. Lee, Appl. Phys. Lett. 85 (2004) 3241.
[7] J.A. Zapien, Y. Jiang, X.M. Meng, W. Chen, F.C.K. Au, Y. Lifshitz, S.T. Lee, Appl. Phys. Lett. 84 (2004) 1189.
[8] M. Ueta, H.B. Kanzaki, K. Kobayashi, Y. Toyozawa, E. Hanamura, Excitonic Processes in Solids, in: Springer Series in Solid State Sciences, vol. 60, Springer, Berlin, 1986.
[9] R.A.M. Hikmet, V. Talapin, H. Weller, J. Appl. Phys. 93 (2003) 3509.
[10] N. Murase, R. Jagannathan, Y. Kanematsu, M. Watanabe, A. Kurita, K.H. Irata, T. Yazawa, T. Kushida, J. Phys. Chem. B 103 (1999) 754.
[11] I. Yu, T. Isobe, M. Senna, J. Phys. Chem. Solids 57 (1996) 373.
[12] K. Sooklal, B.S. Cullum, S.M. Angel, C.J. Murphy, J. Phys. Chem. 100 (1996) 4551.
[13] H. Zhou, D. Hofmann, H.R. Alves, Bruno K. Meyer, J. Appl. Phys. 99 (2006) 103502.
[14] M. Marandi, N. Taghavinia, Z. Sedeghat, A. Irajizad, S.M. Mahdavi, Nanotechnology 19 (2008) 225705.
[15] M.A. Chamarro, V. Voliotis, R. Grousson, P. Lavallard, T. Gacoin, G. Counio, J.-P. Boilot, R. Cases, J. Cryst. Growth 159 (1996) 853.
[16] A. Nag, R. Cherian, P. Mahadevan, A.V. Gopal, A. Hazarika, A. Mohan, A.S. Vengurlekar, D.D. Sarma, J. Phys. Chem. C 114 (2010) 18323.
[17] A. Nag, D.D. Sarma, J. Phys. Chem. C: Lett. 111 (2007) 13641.

[18] A.I. Savchuk, G.Yu. Rudko, V.I. Fediv, A.G. Voloshchuk, E.G. Gule, S.A. Ivanchak, V.V. Makoviy, Phys. Status Solidi C 7 (2010) 1510.
[19] S. Salimian, S.F. Shayesteh, Acta Phys. Pol. A 118 (2010) 633.
[20] B. Tripathi, F. Singh, D.K. Avasthi, D. Das, Y.K. Vijay, Physica B 400 (2007) 70.
[21] S. Bhushan, S.K. Sharma, J. Phys.: Condens. Matter. 2 (1990) 1827.
[22] C.E. Reed, C.G. Scott, Br. J. Appl. Phys. 1 (1968) 1125.
[23] S.K. Mishra, R.K. Srivastava, S.G. Prakash, R.S. Yadav, A.C. Panday, Opto-Electron. Rev. 18 (2010) 467.
[24] N. Badera, B. Godbole, S.B. Srivastava, P.N. Vishwakarma, L.S. Sharath Chandra, D. Jain, M. Gangrade, T. Shripathi, V.G. Sathe, V. Ganesan, Appl. Surf. Sci. 254 (2008) 7042.
[25] J.G. Winiarz, L. Zhang, M. Lal, C.S. Friend, P.N. Prasad, Chem. Phys. 245 (1999) 417.
[26] J.S. Jie, W.J. Zhang, Y. Jiang, X.M. Meng, Y.Q. Li, S.T. Lee, Nano Lett. 6 (2006) 1887.
[27] J. Nanda, K.S. Narayan, B.A. Kuruvilla, G.L. Murthy, D.D. Sharma, Appl. Phys. Lett. 72 (1998) 1335.
[28] J.W. Orton, B.J. Goldsmith, J.A. Chapman, M.J. Powel, J. Appl. Phys. 53 (1982) 1602–1614.
[29] S.E. Ahn, H.S. Lee, H. Kim, S. Kim, B.K. Kang, K.H. Kim, G.T. Kim, Appl. Phys. Lett. 84 (2004) 5022.
[30] S.E. Ahn, H.J. Ji, K. Kim, G.T. Kim, C.H. Bae, S.M. Park, Y.K. Kim, J.S. Ha, Appl. Phys. Lett. 90 (2007) 153106.
[31] A. Bera, D. Basak, Appl. Phys. Lett. 93 (2008) 053102.
[32] A. Bera, D. Basak, Appl. Phys. Lett. 94 (2009) 163119.
[33] L. Peng, J. Li Zhai, D.-J. Wang, P. Wang, Y. Zhang, S. Pang, T.-F. Xie, Chem. Phys. Lett. 456 (2008) 231.
[34] X.Q. Fu, Wang, P. Feng, T.H. Wang, Appl. Phys. Lett. 91 (2007) 073104.
[35] S. Panigrahi, A. Bera, D. Basak, Appl. Mater. Interfaces 1 (2009) 2408.
[36] A. Bera, D. Basak, Appl. Mater. Interfaces 1 (2009) 2066.
[37] R. Kripal, A.K. Gupta, R.K. Srivastava, S.K. Mishra, Spectrochim. Acta A 79 (2011) 1605.
[38] A. Maurya, P. Chauhan, S.K. Mishra, R.K. Srivastava, J. Alloys Compd. 509 (2011) 8433.
[39] Z. Sedaghat, N. Tagavinia, M. Marandi, Nanotechnology 17 (2006) 3812.
[40] Y. Wang, N. Herron, J. Phys. Chem. 95 (1991) 525.
[41] B.A. Simmons, S. Li, V.T. John, G.L. McPherson, A. Bose, W. Zhou, J. He, Nano Lett. 2 (2002) 263.
[42] S. Sadhu, P.S. Chodhury, A. Patra, J. Lumin. 126 (2007) 387.
[43] B.D. Culty, Elements of X-ray Diffraction, Addision-Wesley, New York, 1978.
[44] R. Banerjee, R. Jayakrishnan, P. Ayyub, J. Phys.: Condens. Matter. 12 (2000) 10647.
[45] A. Goswami, Thin Film Fundamentals, New Age International Publishers, New Delhi, India, 2007, p. 69.
[46] V. Singh, P.K. Sharma, P. Chauhan, Mater. Charact. 62 (2011) 43.
[47] J.I. Pankove, Optical Processes in Semiconductors, Prentice-Hall, Englewood Cliffs, NJ, 1971.
[48] L.E. Brus, J. Chem. Phys. 80 (1984) 4403.
[49] L.E. Brus, J. Chem. Phys. 79 (1983) 5566.
[50] B. Zhou, Z. Liu, H. Wang, Y. Yang, W. Su, Catal. Lett. 132 (2009) 75.
[51] C. Wang, H.M. Wang, Z.Y. Fang, J. Alloys Compd. 486 (2009) 702.
[52] A. Nag, S. Sapra, S.S. Gupta, A. Prakash, A. Ghangrekar, N. Periasamy, D.D. Sharma, Bull. Mater. Sci. 31 (2008) 561.
[53] S. Chadramohan, A. Kanjilal, J.K. Tripathi, S.N. Sarangi, R. Sathyamoorthy, T. Som, J. Appl. Phys. 105 (2009) 123507.
[54] Y. Kanemistu, H. Matshbara, C.W. White, Appl. Phys. Lett. 81 (2002) 535.
[55] S. Taguchi, A. Ishizumi, T. Tayagaki, Y. Kanemitsu, Appl. Phys. Lett. 94 (2009) 173101.
[56] R.W. Smith, A. Rose, Phys. Rev. 97 (1955) 1531.
[57] R.H. Bube, Photoconductivity of Solids, John Wiley, New York, 1967, p. 404.
[58] O. Vigil, E. Vasco, O. Zelaya-Angel, Matter. Lett. 29 (1996) 107.
[59] D.H. Zhang, D.E. Brodie, Thin Solid Films 261 (1995) 334.
[60] X.G. Zheng, Q.Sh. Li, W. Hu, D. Chen, N. Zhang, M.J. Shi, J.J. Wang, L.Ch. Zhang, J. Lumin. 123 (2007) 198.
[61] S.K. Mishra, R.K. Srivastava, S.G. Prakash, R.S. Yadav, A.C. Pandey, Elect. Mater. Lett. 7 (2011) 31.
[62] A. Nag, S. Sapra, C. Nagamani, A. Sharma, N. Pradhan, S.V. Bhat, D.D. Sharma, Chem. Mater. 19 (2007) 3252.
[63] R.S. Yadav, R. Mishra, A.C. Pandey, J. Exp. Nanosci. 4 (2009) 139.